Soft Matter

Accepted Manuscript

ROYAL SOCIETY OF CHEMISTRY

www.rsc.org/softmatter

Journal Name

RSCPublishing

ARTICLE

Noncovalent fabrication and tunable fusion of block copolymer-giant polyoxometalate hybrid micelles

Cite this: DOI: 10.1039/x0xx00000x

Liying Zhang, Haolong Li* and Lixin Wu*

Received 00th January 2012,
Accepted 00th January 2012

DOI: 10.1039/x0xx00000x

www.rsc.org/

The block copolymers (BCs), as structure-directing agents, coassembling with nanoscale inorganic additives is an important route to fabricate nanostructured hybrid materials. In this work, we present a facile approach to fabricate hybrid micelles composed of BCs and polyoxometalates (POMs), in which the POM clusters are premodified with the groups that can specifically interact with a certain BC block. A representative POM $(NH_4)_{42}[Mo_{132}O_{372}(CH_3COO)_{30}(H_2O)_{72}]$ (Mo_{132}) is chosen as the example and encapsulated with cationic molecules containing carboxyphenyl groups through electrostatic interaction, and then the resulting hybrid complex can further coassemble with poly(styrene-*block*-4-vinylpyridine) (PS-*b*-P4VP) through hydrogen bond with the pyridine groups, which leads to the formation of hybrid micelles and the localization of Mo_{132} in the micelle cores. The micelles exhibit a high stability despite of time and dilution. Furthermore, the fusion of the micelles can be readily adjusted by varying the length of PS blocks, which is promising to be used in constructing polymer-POM hybrid materials with discrete or continuous hybrid domains. This work is based on the electrostatic premodification of POMs and thus its concept is generally suitable for the whole anionic POM system, which may create a large class of BC/POM nanocomposites with tunable structures.

Introduction

In the past few decades, the self-assembly of block copolymers (BCs) has attracted considerable attention owning to their diverse phase separation morphologies in solution and solid state,[1,2] which provides excellent templates for organizing nanoscale inorganic additives such as metal and semiconductor nanoparticles as well as clusters to fabricate nanostructured hybrid materials.[3–9] Selective localization of inorganic additives in specific domains of ordered BCs assemblies significantly influences the properties and potential applications of the resulting hybrid materials.[10,11] In this context, efficient strategies for controllable coassembly of BCs with different inorganic additives are highly desired.

Polyoxometalates (POMs) are nanoscale discrete metal-oxide clusters with a large compositional and structural diversity, and they exhibit abundant properties in catalysis, optics, magnetics and electronics.[12–15] POMs are widely employed as versatile inorganic building blocks for fabricating hybrid materials, in particular hybridization with polymers.[16,17] The incorporation and dispersion of POMs in polymer matrix like monoliths and latex spheres has been realized through a post-functionalization procedure of POMs and their subsequent copolymerization with monomers.[18–21] However, the selective localization of POMs in certain polymer domains is still a challenge due to the difficulty in attaining a specific interaction between POMs and polymer chains. To address this issue, it is advisable to appeal the assistance of BCs as structure-directing agents.

In the recent five years, several instances have been reported to coassemble POMs with BCs through electrostatic interaction, which lead to various hybrid nanostructures, including spherical micelles,[22–24] cylindrical micelles,[24] vesicles,[22,23,25,26] nanosheets[25] and bicontinuous networks.[26] The general principle of these works depends on the ionic complexation of negatively charged POM clusters with the positively charged blocks of BCs. The phase separation of BC chains directs the localization of binded POMs. However, electrostatic interaction has its intrinsic limitation, for example it needs the BCs containing a cationic block and a high polar environment to carry out the counterion exchange between BCs and POMs. Therefore, it is necessary to apply other driving forces as alternatives to coassemble BCs with POMs.

The post-functionalization chemistry of POMs allows the modification of different organic groups onto the framework or surface of POMs.[27,28] Particularly, electrostatic encapsulation with cationic organic molecules is generally suitable for the whole anionic POM system, which can offer a large class of hybrid complex with flexibly adjusted organic motifs.[29,30] Our

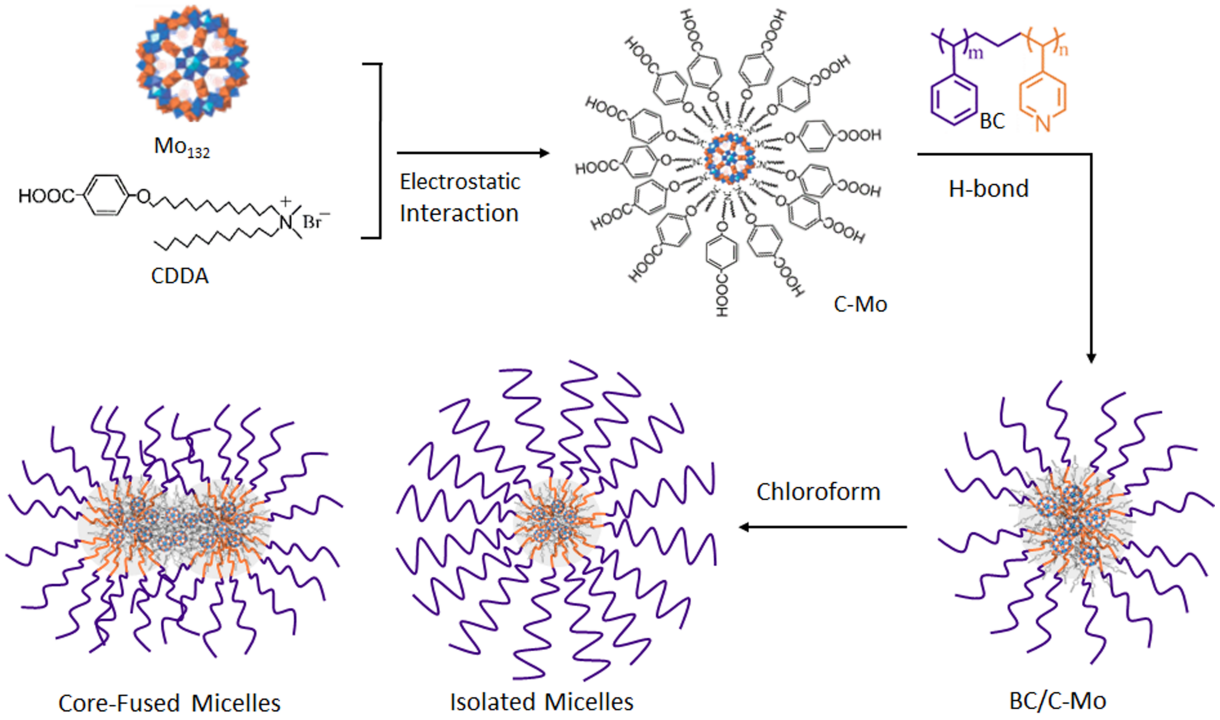

Scheme 1 Schematic representation of the fabrication route of PS-*b*-P4VP/ C-Mo nanacomposite micelles.

group focuses on the self-assembly and functionalization of electrostatically modified POMs,[31–35] and has introduced POMs into homopolymer matrix and silica networks by using the modified groups as linkers.[19–21,36] In this work, we extend this concept to the fabrication of BC/POM nanocomposites in which the POM is premodified with the groups that can specifically interact with certain block of BC through noncovalent interaction. Following this idea, we designed a dual functional molecule N-[12-(4-carboxylpheny)dodecyloxyl]-N-dodecyl-N,N-dimethyla-mmonium bromide (noted as CDDA), as shown in Scheme 1, which contains both a quaternary ammonium group and a carboxyphenyl group on its two terminals. When using CDDA to encapsulate a representative highly charged POM $(NH4)_{42}[Mo_{132}O_{372}(CH_3COO)_{30}(H_2O)_{72}]$ (noted as Mo132),[37] a hybrid complex with abundant carboxyphenyl groups on the periphery was obtained. The complex could coassemble with poly(styrene-*block*-4-vinylpyridine) (noted as PS-*b*-P4VP) to form hybrid micelles through hydrogen bond. Furthermore, the fusion of the micelles was readily adjusted by varying the length of PS blocks. This work provides a facile and general approach to selectively localize POM clusters in BC matrix.

Results and discussion

Structural characterization of C-Mo complex

In our study, the quaternary ammonium group of CDDA interacts with Mo_{132} through electrostatic interaction, which forms a organic-inorganic complex (noted as C-Mo) by a widely used "phase transfer" method.[29,30] After encapsulating Mo_{132} with CDDA, the resulting complex are not soluble in water like pristine Mo_{132}, but soluble in low polar solvents like tetrahydrofuran, which indicates the hydrophilic surface of Mo_{132} has been efficiently encapsulated by hydrophobic CDDA. The detailed preparation process is described in Experimental Section. The C-Mo was characterized by IR spectrum and elemental analysis. From IR spectrum (Fig. 1) and its assignments of spectral peaks (Table 1), the characteristic Mo-O stretching vibration bands of Mo_{132} (Fig. 1a) also appear in the IR spectrum of C-Mo (Fig. 1b) at 982, 951, 860, 806 and 733 cm^{-1}. This result implies that the metal-oxygen framework of Mo_{132} is well retained in C-Mo. On the other hand, the asymmetrical and symmetrical stretching bands of CH_2 group are observed in the IR spectrum of C-Mo at 2922 and 2852 cm^{-1}, similar to those bands of pristine CDDA appearing at 2922 and 2851 cm^{-1} (Fig. 1c), which indicates that the alkyl chains are intact in C-Mo. Furthermore, the average number of CDDA on one Mo_{132} is 41, according to the elemental analysis results (Table S1). Therefore, the chemical formula of C-Mo is $(CDDA)_{41}(NH_4)Mo_{132}$.

Fabrication of PS-*b*-P4VP/C-Mo nanocomposites

The PS-*b*-P4VP/C-Mo nanocomposites were prepared through mixing a series of four kinds of PS-*b*-P4VP and C-Mo in tetrahydrofuran/chloroform mixed solvent and then evaporating the solvent. The details are described in the Experimental Section. The employed PS-*b*-P4VP contains almost the same

length of P4VP blocks but different lengths of PS blocks, which are noted as PS9.8, PS24, PS47 and PS310 according to the molar mass of PS blocks. In the nanocomposites, the carboxyphenyl group of CDDA interacts with the pyridine group of PS-*b*-P4VP through hydrogen bond. The molar ratio of carboxyphenyl group to pyridine group (noted as *r*) was controlled to be 0.3 to insure the high loading weight of Mo_{132} in nanocomposites. When *r* is above 0.3, PS9.8/C-Mo are not soluble in tetrahydrofuran/chloroform mixed solvent. However, the other three nanocomposites, PS24/C-Mo, PS47/C-Mo and PS310/C-Mo, retain good solubility when *r* is above 0.3 in the same mixed solvent. For PS310/C-Mo, no precipitates were observed after 10 days when *r* reaches to 0.8.

After removing the mixed solvent, IR is used to confirm the hydrogen bond of PS-*b*-P4VP/C-Mo nanocomposites in the solid state, as shown in Fig. S1. For pristine C-Mo, an absorption band appears at 1683 cm^{-1}, which is assigned to C=O stretching mode; meanwhile, the weak double absorption bands at 2557 and 2669 cm^{-1} represent the formation of hydrogen bond, which imply that the terminal carboxyphenyl groups exist in the intermolecular cyclic dimer state definitely.[38] For PS9.8/C-Mo, we found the characteristic vibration bands at about 1703 cm^{-1} deriving from carbonyl stretching, which confirms that the hydrogen bond occurs between the carboxyphenyl group of C-Mo and the pyridine group of PS9.8. For PS24/C-Mo and PS47/C-Mo, the similar shifts of carbonyl stretching are observed. However, for PS310/C-Mo, because of the high contain of PS in nanocomposites, the IR bands of PS at 1700 nm^{-1} overlap the carbonyl stretching peak. However, the ^1H NMR spectrum of PS310/C-Mo in $CDCl_3$ demonstrates the existence of hydrogen bond between PS310 and C-Mo, as shown in Fig. 2A.

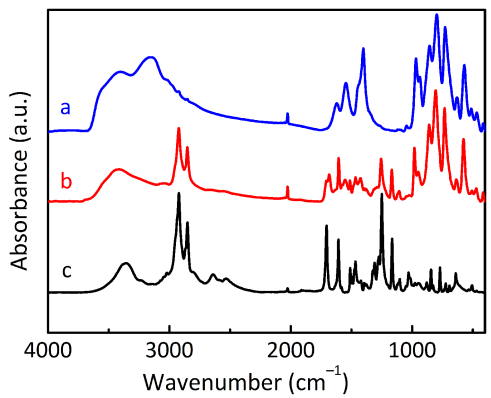

Fig. 1 FT-IR spectra of (a) Mo_{132}, (b) C-Mo, and (c) CDDA in KBr pellets.

Table 1. Assignments [a] of the characteristic IR vibration bands (cm^{-1}) of Mo_{132}, C-Mo and CDDA.

Mo_{132}	C-Mo	CDDA	Assignments
—	2922	2922	$\nu_{as}(CH_2)$
—	2852	2851	$\nu_s(CH_2)$
—	1466	1468	$\delta(CH_2)$
969, 937	982, 951	—	ν(Mo=O)
856, 798, 727	860, 806, 733	—	ν_{as}(Mo-O-Mo)

[a] ν_{as}: asymmetrical stretching; ν_s: symmetrical stretching; δ: scissoring stretching; ν: stretching.

Structural characterization of PS-*b*-P4VP/C-Mo nanocomposite micelles

As chloroform is a non-selective solvent for PS-*b*-P4VP and is a poor solvent for C-Mo, it was chosen to redisperse the four kinds of PS-*b*-P4VP/C-Mo nanocomposites to obtain their micelles. The solubility of PS9.8/C-Mo in chloroform is very poor due to the short PS block length and only a heterogeneous suspension can be formed, while PS24/C-Mo, PS47/C-Mo and PS310/C-Mo are well soluble in chloroform.

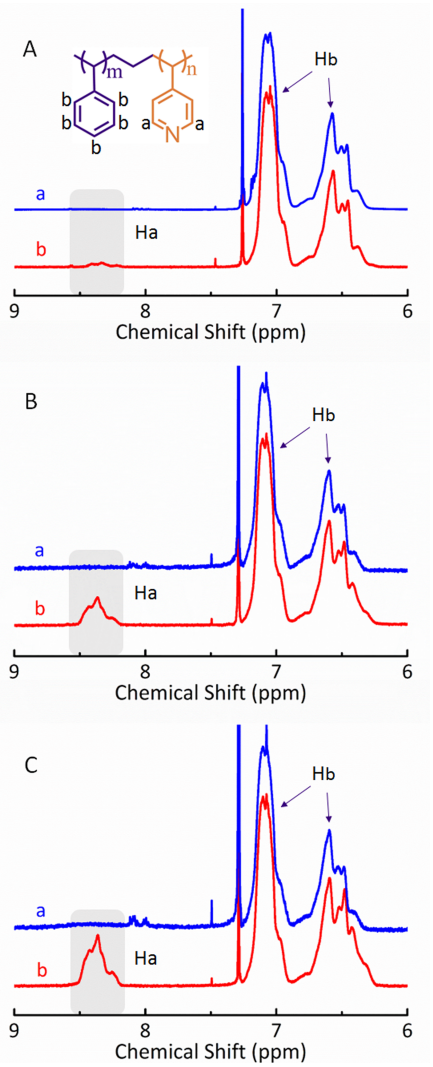

Fig. 2 ^1H NMR spectra of (a) PS310/C-Mo and (b) PS310 in A, (a) PS47/C-Mo and (b) PS47 in B and (a) PS24/C-Mo and (b) PS24 in C in $CDCl_3$.

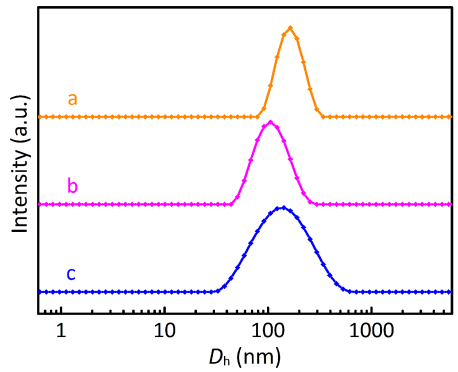

Fig. 3 DLS diagram of (a) PS310/C-Mo, (b) PS47/C-Mo and (c) PS24/C-Mo in chloroform.

^{1}H NMR spectroscopy was used to confirm the in-situ hydrogen bonding interaction in PS-*b*-P4VP/C-Mo nanocomposites in solution. In Fig. 2, the grey part ranging from 8.2 ppm to 8.6 ppm represents the two aromatic pyridyl protons (Ha) from the P4VP block, while the signals ranging from 6.3 ppm to 7.2 ppm belong to the aromatic protons (Hb) of PS block. For a convenient comparison, the PS signals are adjusted to similar intensities. With the increase of the molar ratio of PS against P4VP, the Ha signals gradually become stronger from PS310/C-Mo, PS47/C-Mo, to PS24/C-Mo, as shown in Fig. 2A, Fig. 2B and Fig. 2C, respectively. The ^{1}H NMR spectra of PS310/C-Mo and pristine PS310 (Fig. 2A) were taken as a pair of representative examples for detailed discussion. Compared with PS310 (b), the intensity of peaks attributed to Ha of PS310/C-Mo (a) weaken obviously, which can be explained in terms of the lower shielding effect and the limited mobility of pyridine group induced by hydrogen bond. For PS47/C-Mo and PS24/C-Mo, the similar phenomena of weakening Ha signals are observed in Fig. 2B and Fig. 2C, respectively. These results demonstrate that the formation of hydrogen bond between the pyridine groups from P4VP block and the carboxyphenyl groups from C-Mo in the nanocomposites in chloroform.

To reveal the structure information of PS-*b*-P4VP/C-Mo assemblies in chloroform, we firstly used dynamic light scattering (DLS) method to analyse the hydrodynamic diameter (D_h) of assemblies. As the solubility of PS9.8/C-Mo in chloroform is poor, it can only form a suspension containing very large particles that are not suitable for DLS characterization. The other three nanocomposites can give reasonable DLS diagrams, as shown in Fig. 3 and Table S2. The PS310/C-Mo (a) exhibits only one peak at about 157 nm and its PDI is 0.057, which indicates a uniform spherical structure. For the PS47/C-Mo (b), there is also only one peak with the PDI of 0.100, which means the structure should be uniform spherical assembly. Moreover, the peak appearing at about 101 nm reveals that the D_h of PS47/C-Mo is smaller than PS310/C-Mo`s. This result is consistent with the fact that the molecular length of PS310 is longer than PS47 when we control them with the same P4VP length and C-Mo loading weight by controlling r to be 0.3. Interestingly, for the PS24/C-Mo (c) there is a broad peak at about 120 nm whose PDI is 0.233, which suggests that the assemblies should be nonuniform or even not spherical. Because the structure information obtained from DLS is limited, we further characterize the PS-*b*-P4VP/C-Mo assemblies by atomic force microscope (AFM) and transmission electron microscope (TEM).

The height image of AFM offers the morphology information of the nanocomposite assemblies, as shown in Fig. 4. Most of the PS310/C-Mo assemblies are isolated spherical assemblies, their diameter and height are about 140.6 nm and 9.6 nm,

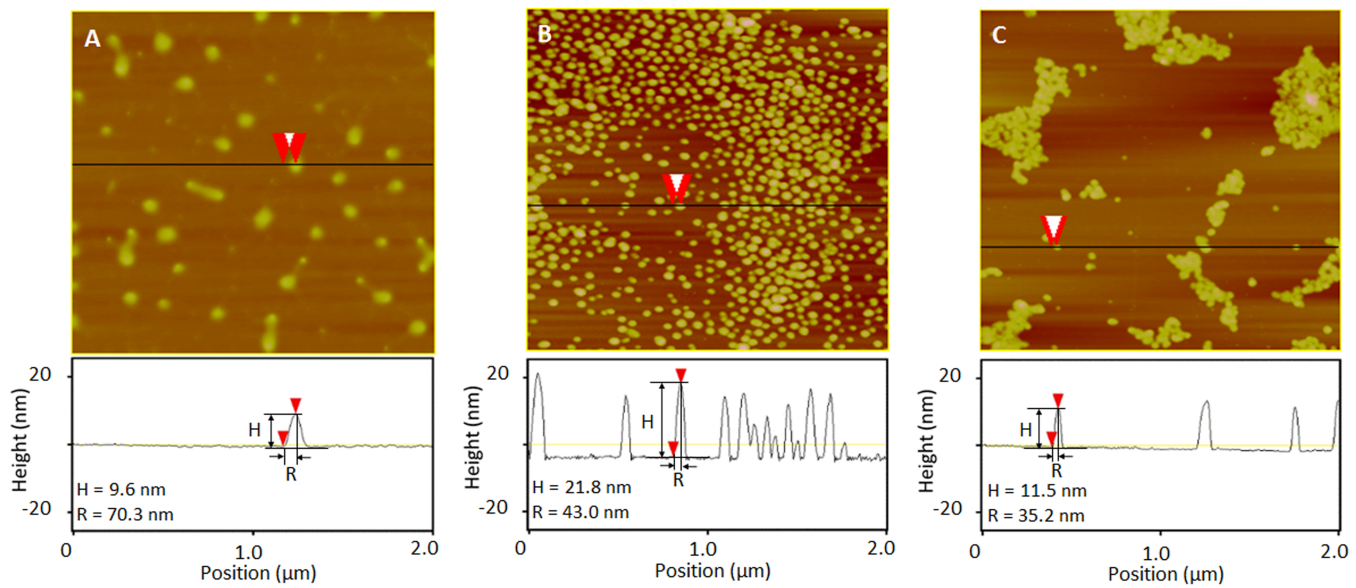

Fig. 4 AFM height images (up) and corresponding height profiles (down) of (A) PS310/C-Mo, (B) PS47/C-Mo and (C) PS24/C-Mo.

respectively (Fig. 4A). The diameter is a little smaller than the D_h from DLS, which should be due to the shrinking effect of the assemblies after solvent evaporation. The diameter is much larger than the height because of the flexible property of PS corona leading to a flattened morphology of the micelles. For PS47/C-Mo (Fig. 4B), the assemblies are also isolated and

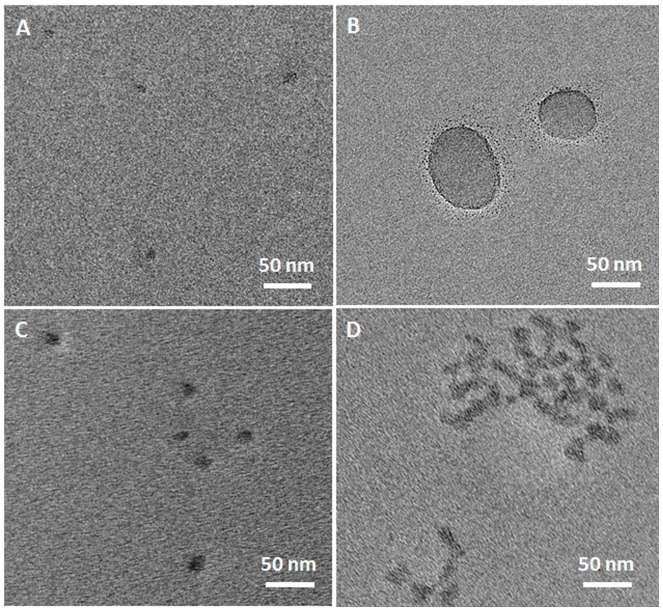

Fig. 5 TEM images of (A) PS310/C-Mo and (B) staining by RuO_4, (C) PS47/C-Mo and (D) PS24/C-Mo.

flattened spheres, the diameter and height are about 86.0 nm and 21.8 nm, respectively. However, for PS24/C-Mo (Fig. 4C), most of the assemblies are aggregated and only a few of them are isolated spherical assemblies whose diameter and height are about 70.4 nm and 11.5 nm, also showing a flattened structure. For PS9.8/C-Mo (Fig. S3), almost all the assemblies are aggregated, which is consistent with their poor solubility in chloroform.

TEM measurement was further used to clarify the inner structure of the nanocomposite assemblies, which is the insoluble P4VP/C-Mo domain. Mo_{132} clusters contain heavy metals and thus show a strong electron scattering in TEM observation, while PS blocks are not visible. Thus, the dark regions in TEM images correspond to the P4VP/C-Mo domain. For PS310/C-Mo (Fig. 5A), isolated dark dots with the average diameters of about 11 nm are observed (Fig. S5A), which are much smaller than the whole size of assemblies measured by AFM, indicating that the PS310/C-Mo nanocomposites assembled into core-corona spherical micelles whose core is formed by P4VP and C-Mo through hydrogen bond and corona is formed by PS. After staining by RuO_4, the PS corona of PS310/C-Mo appears in TEM images (Fig. 5B), further confirming the core-corona structure. The isolated core of PS47/C-Mo assemblies (Fig. 5C) shows an average diameter of about 14 nm (Fig. S5B). This value is a little larger than that of PS310/C-Mo core, because the high density of PS corona of

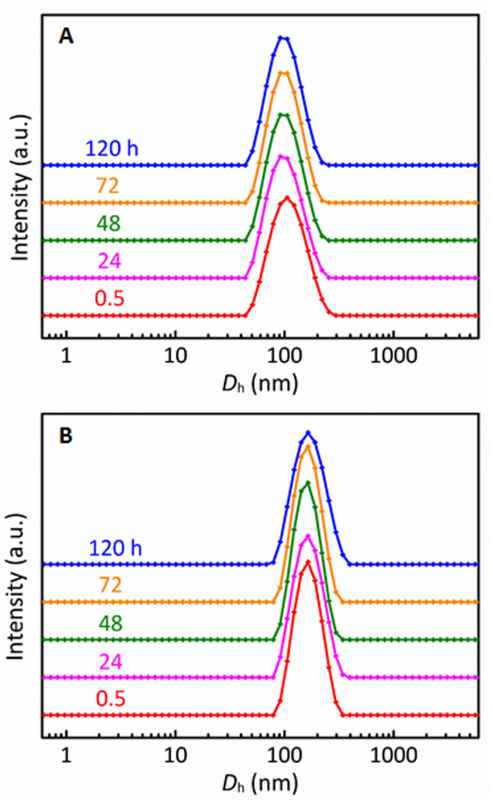

Fig. 6 DLS diagrams of (A) PS310/C-Mo and (B) PS47/C-Mo at different times after preparation in chloroform.

PS310/C-Mo induces a high repulsive force which leads to smaller core size. However, for PS24/C-Mo, only a few cores are isolated and most of them are fused to form a network-like structure, as shown in Fig. 5D, which is in consistent with its AFM images. The network-like structures of PS24/C-Mo are gradually fused from isolated micelles (Fig. S7A) to slightly linked micelles (Fig. S7B) then to the final micelle networks (Fig. S7C). The RuO_4 staining effects of the PS part of PS47/C-Mo and PS24/C-Mo are not very obvious (Fig. S6), due to the decreased PS content in comparison with the hybrid domains. For PS9.8/C-Mo, the core fusion become more serious and the dark region are completely linked to network structure (Fig. S4). We presumed that the fused cores of P4VP/C-Mo domain observed in PS9.8/C-Mo and PS24/C-Mo nanocomposites result from the low PS density, which is not adequate to prevent the inter-micelle hydrogen bonding interaction. Therefore, it is reasonable to comprehend that the fused cores are less when increasing the density of PS corona. From the experiment point of view, it is readily to vary the PS density by controlling the length of PS blocks, which can provide a facile route to adjust the distribution state of Mo_{132} hybrid domains in polymer matrix, for example from discrete to continuous phase. This concept is promising to be extended to other BC/POM systems and may find potential applications in the fabrication of cluster hybrid materials or devices with precisely adjustable properties. We further use DLS to investigate the stability of the isolated PS-*b*-P4VP/C-Mo micelles. The size distribution of PS47/C-

Mo and PS310/C-Mo are both retained at the same position after 120 h since preparation (Fig. 6) or after decreasing their concentration to 2×10^{-8} mol/L regarding polymer part in Fig. S2, which confirms the high stability of the micelles. Therefore, these nanocomposite micelles are suitable to be used as building blocks for the hierarchical assembly of ordered polymer-POM hybrid materials.

Conclusions

We present a facile and general route to fabricate the hybrid micelles composed of BCs and POMs. In this route, the POM clusters such as Mo_{132} are electrostatically premodified with carboxyphenyl groups which is a hydrogen bond donor, and then the formed complex further interact with the pyridine groups of PS-*b*-P4VP through hydrogen bond, thus realizing the localization of Mo_{132} in the core of hybrid BC micelles. The micelles exhibits a high stability despite of preparation time and dilution. Interestingly, the core-fusion of the micelles can be readily adjusted by varying the length of PS blocks, which may develop potential applications in the preparation of polymer-POM hybrid materials with discrete or continuous hybrid domains. In comparison with the conventional way that coassembling BCs with bare POM clusters through ionic bond, the concept in present route based on the electrostatic premodification of POMs is more generally suitable for the whole anionic POM system. Moreover, in principle, the modified groups can be extended to those can provide other noncovalent interactions with BC blocks, for example polymer chains with the same chemical composition of certain block of BC matrix may offer an enthalpy-driven interaction, which is promising to create a large class of BC/POM nanocomposites with tunable structures.

Experimental

Materials

Mo_{132} were synthesized according to the literature.[37] CDDA was synthesized as literature.[38] Four kinds of PS-*b*-P4VP were all commercial products from Polymer Source Inc. and used as received. PS_{94}-*b*-$P4VP_{95}$ (the subscripts refer to the degree of polymerization) is denoted as PS9.8 whose molecular weight is 9.8-*b*-10×10^3 kg/mol and PDI is 1.08; PS_{230}-*b*-$P4VP_{90}$ is denoted as PS24 whose molecular weight is 24-*b*-9.5×10^3 kg/mol and PDI is 1.10; PS_{448}-*b*-$P4VP_{95}$ is denoted as PS47 whose molecular weight is 47-*b*-10×10^3 kg/mol and PDI is 1.10; PS_{2952}-*b*-$P4VP_{95}$ is denoted as PS310 whose molecular weight is 310-*b*-10×10^3 kg/mol and PDI is 1.09. Chloroform and tetrahydrofuran were purchased from Beijing chemical works and were distilled before using.

Preparation of C-Mo

The CDDA encapsulated Mo_{132} complex (C-Mo) was prepared following the procedure reported previously.[29,30] Mo_{132} was dissolved in water, and then a chloroform solution of CDDA was added with stirring. The initial molar ratio of CDDA to Mo_{132} was controlled at 38:1. The colour of water phase became colourless from dark reddish brown. The formed C-Mo was not soluble in water or chloroform and thus precipitated from phase separated solvents. The complex was obtained by filtering the solvent and washing by water twice and chloroform twice. The sample was further dried under vacuum until its weight remained constant. The product were characterized by IR and elemental analysis.

Preparation of PS-*b*-P4VP/C-Mo nanocomposite micelles

The nanocomposite micelles based on PS-*b*-P4VP and C-Mo were prepared by the following procedure, as exemplified by PS310/C-Mo. C-Mo was dissolved in tetrahydrofuran and PS310 was dissolved in chloroform. Then to the PS310 solution, a C-Mo solution was added with stirring when r is 0.3. After stirring for 0.5 hour, the sample was ultrosonicated for 5 min, and then the PS310/C-Mo nanocomposite was obtained. The product was redispersed in chloroform to obtain hybrid micelles. The concentration of PS310 in chloroform is 2×10^{-6} mol/L. The other three nancomposites were prepared by similar procedures. The nanocomposite micelles were characterized by IR, ^{1}H NMR, DLS, AFM and TEM in detail.

Measurements

FT-IR spectra were collected on a Bruker Vertex 80v spectrometer equipped with a deuterated triglycine sulphate (TGS) detector (32 scans) for pressed KBr pellets and mercury cadmium telluride (MCT) detector (512 scans) for CaF_2 substrates with a resolution of 4 cm^{-1}. ^{1}H NMR spectra (with tetramethylsilane as reference) were recorded on a Bruker UltraShield 500 MHz spectrometer using $CDCl_3$ as solvent. Organic elemental analysis (C H N) was performed on a Flash EA1112 from TherMoQuest Italia S.P.A. Dynamic light scattering (DLS) measurements were performed by using a Malvern Zetasizer NanoZS instrument at room temperature in chloroform solution with the concentration is 2×10^{-6} mol/L regarding the polymer part. AFM images were measured on a Bruker Dimension 3100 instrument with tapping mode in air. The AFM height images were minimally flattened, and a single low-pass filter for diminishing high-frequency noise was applied to facilitate data analysis. AFM samples were prepared by spin-coating the chloroform solution of nanocomposites onto Si substrates at 400 rpm for 30 s and then 1500 rpm for 60 s. For PS310/C-Mo, we dilute its solution to 2×10^{-7} mol/L before spin-coating. TEM images were obtained with a JEM-2100F electron microscope operating at 200 kV. TEM samples are prepared by casting the chloroform solution of nanocomposites onto carbon-coated copper grids. Before casting, we dilute the solution of PS310/C-Mo to 2×10^{-8} mol/L and PS47/C-Mo to 2×10^{-7} mol/L.

Acknowledgements

We acknowledge the financial supports from the National Basic Research Program (2013CB834503), National Natural Science

Foundation of China (91227110, 21221063 and 21274053), and the Open Project of State Key Laboratory of Polymer Physics & Chemistry of CAS.

Notes and references

State Key Laboratory of Supramolecular Structure and Materials, College of Chemistry, Jilin University, Changchun 130012, China.
* Corresponding author. E-mail: hl_li@jlu.edu.cn; wulx@jlu.edu.cn

Electronic Supplementary Information (ESI) available: elemental analysis results of C-Mo, FT-IR spectra and DLS data of four kinds of PS-*b*-P4VP/C-Mo, DLS diagrams of PS47/C-Mo and PS310/C-Mo in diluted chloroform solution, AFM images and TEM images of PS9.8/C-Mo, core diameter distribution histograms and corresponding Gaussian fits of PS310/C-Mo and PS47/C-Mo, TEM images of PS47/C-Mo and PS24/C-Mo after RuO_4 staining and TEM images of PS24/C-Mo at different intermediate states. See DOI: 10.1039/b000000x/

1 M. Moffitt, K. Khougaz and A. Eisenberg, *Acc. Chem. Res.*, 1996, **29**, 95–102.
2 C. Park, J. Yoon and E. L. Thomas, *Polymer*, 2003, **44**, 6725–6760.
3 S. Förster and M. Antonietti, *Adv. Mater.*, 1998, **10**, 195–217.
4 M. R. Bockstaller, R. A. Mickiewicz and E. L. Thomas, *Adv. Mater.* 2005, **17**, 1331–1349.
5 A. C. Balazs, T. Emrick and T. P. Russell, *Science*, 2006, **314**, 1107–1110.
6 J. Yuan and A. H. E. Müller, *Polymer*, 2010, **51**, 4015–4036.
7 M. C. Orilall and U. Wiesner, *Chem. Soc. Rev.*, 2011, **40**, 520–535.
8 S. G. Jang, E. J. Kramer and C. J. Hawker, *J. Am. Chem. Soc.*, 2011, **133**, 16986–16996.
9 Y. Zhao, K. Thorkelsson, A. J. Mastroianni, T. Schilling, J. M. Luther, B. J. Rancatore, K. Matsunaga, H. Jinnai, Y. Wu, D. Poulsen, J. M. J. Fréchet and A. P. Alivisatos, T. Xu, *Nature Mater.*, 2009, **8**, 979–985.
10 Y. Mai and A. Eisenberg, *Acc. Chem. Res.*, 2012, **45**, 1657–1666.
11 J. Kao, K. Thorkelsson, P. Bai, B. J. Rancatore and T. Xu, *Chem. Soc. Rev.*, 2013, **42**, 2654–2678.
12 M. T. Pope and A. Müller, *Angew. Chem., Int. Ed. Engl.*, 1991, **30**, 34–48.
13 *Special Thematic Issue on Polyoxometalates*, ed. C. L. Hill, *Chem. Rev.* 1998, **98**, 1–390.
14 *Thematic Issue on Polyoxometalate Cluster Science*, ed. L. Cronin and A. Müller, *Chem. Soc. Rev.*, 2012, **41**, 7325–7648.
15 D.-L. Long, R. Tsunashima and L. Cronin, *Angew. Chem., Int. Ed.*, 2010, **49**, 1736–1758.
16 W. Qi, L. Wu, *Polym. Int.,* 2009, **58**, 1217–1225.
17 Y. Han, Y. Xiao, Z. Zhang, B. Liu, P. Zheng, S. He and W. Wang, *Macromolecules*, 2009, **42**, 6543–6548.
18 C. R. Mayer, V. Cabuil, T. Lalot and R. Thouvenot, *Adv. Mater.*, 2000, **12**, 417–420.
19 H. Li, W. Qi, W. Li, H. Sun, W. Bu, L. Wu, *Adv. Mater.*, 2005, **17**, 2688–2692.
20 H. Li, W. Qi, H. Sun, P. Li, Y. Yang, L. Wu, *Dyes Pigments*, 2008, **79**, 105–110.
21 H. Li, P. Li, Y. Yang, W. Qi, H. Sun and L. Wu, *Macromol. Rapid Commun.*, 2008, **29**, 431–436.
22 W. Bu, S. Uchida and N. Mizuno, *Angew. Chem., Int. Ed.*, 2009, **48**, 8281–8284.
23 Q. Zhang, Y. Liao, L. He and W. Bu, *Langmuir*, 2013, **29**, 4181−4186.
24 X. Lin, F. Liu, H. Li, Y. Yan, L. Bi, W. Bu and L. Wu, *Chem. Commun.*, 2011, **47**, 10019–10021.
25 J. Zhang, Y. Liu, Y. Li, H. Zhao and X. Wan, *Angew. Chem., Int. Ed.*, 2012, **51**, 4598–4602.
26 T. Lunkenbein, M. Kamperman, Z. Li, C. Bojer, M. Drechsler, S. Förster, U. Wiesner, A. H. E. Müller and J. Breu. *J. Am. Chem. Soc.*, 2012, **134**, 12685–12692.
27 A. Dolbecq, E. Dumas, C. R. Mayer and P. Mialane, *Chem. Rev*. 2010, **110**, 6009–6048.
28 A. Proust, B. Matt, R. Villanneau, G. Guillemot, P. Gouzerh and G. Izzet, *Chem. Soc. Rev.*, 2012, **41**, 7605–7622.
29 D. G. Kurth, P. Lehmann, D. Volkmer, H. Cölfen, M. J. Koop, A. Müller and A. D. Chesne, *Chem. Eur. J.*, 2000, **6**, 385–393.
30 D. Volkmer, A. D. Chesne, D. G. Kurth, H. Schnablegger, P. Lehmann, M. J. Koop and A. Müller, *J. Am. Chem. Soc.*, 2000, **122**, 1995–1998.
31 W. Bu, H. Li, H. Sun, S. Yin and L. Wu, *J. Am. Chem. Soc.*, 2005, **127**, 8016–8017.
32 H. Li, H. Sun, W. Qi, M. Xu and L. Wu, *Angew. Chem., Int. Ed.*, 2007, **46**, 1300–1303.
33 Y. Yan, H. Wang, B. Li, G. Hou, Z. Yin, L. Wu and V. W. W. Yam, *Angew. Chem., Int. Ed.*, 2010, **49**, 9233–9236.
34 Y. Wang, H. Li, C. Wu, Y. Yang, L. Shi and L. Wu, *Angew. Chem., Int. Ed.*, 2013, **52**, 4577–4581.
35 Y. Yang, B. Zhang, Y. Wang, L. Yue, W. Li and L. Wu, *J. Am. Chem. Soc.*, 2013, **135**, 14500–14503.
36 W. Qi, H. Li and L. Wu, *Adv. Mater.*, 2007, **19**, 1983–1987.
37 A. Müller, E. Krickemeyer, H. Bögge, M. Schmidtmann and F. Peters, *Angew. Chem., Int. Ed.*, 1998, **37**, 3360–3363.
38 S. Yin, H. Sun, Y. Yan, H. Zhang, W. Li and L. Wu, *J. Colloid Interface Sci.*, 2011, **361**, 548–555.

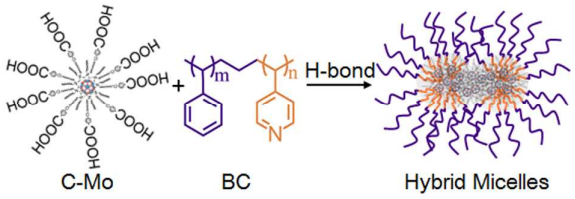

The electrostatically-premodified polyoxometalate clusters are assembled with block copolymers through hydrogen bonding, which forms hybrid micelles with tunable core fusion.